

# A MULTIPLY IMAGED LUMINOUS INFRARED GALAXY BEHIND THE BULLET CLUSTER (1E0657-56)<sup>1</sup>

ANTHONY H. GONZALEZ

Department of Astronomy, University of Florida, Gainesville, FL 32611-2055

DOUGLAS CLOWE

Department of Physics & Astronomy, Ohio University, Clipping Labs 251B, Athens, OH 45701

MARUŠA BRADAČ

Department of Physics, University of California at Santa Barbara, Santa Barbara, CA 93106

DENNIS ZARITSKY

Steward Observatory, University of Arizona, 933 North Cherry Avenue, Tucson, AZ 85721

CHRISTINE JONES AND MAXIM MARKEVITCH

Harvard-Smithsonian Center for Astrophysics, 60 Garden St., Cambridge, MA 02138

*To appear in The Astrophysical Journal*

## ABSTRACT

We present evidence for a *Spitzer*-selected luminous infrared galaxy (LIRG) behind the Bullet Cluster (1E0657-56). The galaxy, originally identified as a multiply imaged source using IRAC photometry, has a spectral energy distribution consistent with a highly extinguished ( $A_V \sim 3.3$ ), strongly star-forming galaxy at  $z = 2.7$ . Using our strong gravitational lensing model presented in Bradač et al. (2006), we find that the magnifications are  $|\mu| \approx 10 - 50$  for the three images of the galaxy. The brightest and faintest images differ by a factor of 3.2 in magnification. The implied infrared luminosity is consistent with the galaxy being a LIRG, with a stellar mass of  $M_* \sim 2 \times 10^{10} M_\odot$  and a star formation rate of  $\sim 90 M_\odot \text{ yr}^{-1}$ . With lensed fluxes at  $24\mu\text{m}$  of 0.58 mJy and 0.39 mJy in the two brightest images, this galaxy presents a unique opportunity for detailed study of an obscured starburst with a star formation rate comparable to that of  $L^*$  galaxies at  $z > 2$ .

*Subject headings:* galaxies: evolution, starburst — gravitational lensing — galaxies: clusters: general

## 1. INTRODUCTION

Measurements of both the star formation history of the universe and corollary build-up of stellar mass have established that the star formation rate peaks at  $1 \lesssim z \lesssim 3$  (e.g. Madau et al. 1996; Lilly et al. 1996; Dickinson et al. 2003; Rudnick et al. 2003; Reddy et al. 2008; Wilkins et al. 2008). *Spitzer*  $24\mu\text{m}$  observations further indicate that star formation at this epoch is dominated by luminous and ultraluminous infrared galaxies (LIRGs and ULIRGs; Pérez-González et al. 2005; Le Floch et al. 2005). ULIRGs are sufficiently bright to facilitate spectroscopy and detailed analyses (Daddi et al. 2005; Yan et al. 2005; Valiante et al. 2007; Pope et al. 2008); however, these galaxies represent only the most massive tail of the galaxy population (Dey et al. 2008; Dye et al. 2008).

In contrast, LIRGs have properties more similar to the overall galaxy population, with stellar masses and star formation rates comparable to those seen for UV-selected star-forming galaxies at  $z \sim 2$  (Reddy & Steidel 2004; Reddy et al. 2006). The intrinsic faintness of LIRGs however precludes both high-fidelity multiwave-

length photometry and spectroscopic programs at optical and infrared wavelengths at  $z \gtrsim 2$ .

Strong gravitational lensing enables observations of intrinsically fainter galaxies than is otherwise possible, and several recent programs have begun to exploit lensing by galaxy clusters to probe the properties of infrared and submillimeter luminous galaxies (e.g. Knudsen et al. 2008; Rigby et al. 2008, and references therein). The main limitation of this approach is simply the small number of known lensed galaxies that are luminous at these wavelengths.

In this paper we present evidence for a strongly lensed, luminous infrared galaxy that is triply imaged by the Bullet Cluster. This galaxy is the only strongly lensed source for which the initial detection was made with *Spitzer* at mid-infrared wavelengths, and due to its large magnification provides a window onto the properties of lower luminosity infrared galaxies than have previously been studied in this redshift regime. In previous papers our team has explored the physical properties of the Bullet Cluster, 1E0657-56, measuring its matter distribution and the properties of the X-ray gas (Markevitch et al. 2002, 2004; Clowe et al. 2004, 2006; Bradač et al. 2006), and constraining the dark matter self-interaction cross-section (Markevitch et al. 2004; Randall et al. 2007). The object that is the subject of this paper was first identified as a doubly lensed source

<sup>1</sup> This paper includes data gathered with the 6.5 meter Magellan Telescopes located at Las Campanas Observatory, Chile, the Hubble Space Telescope, and the Spitzer Space Telescope.  
Electronic address: anthony@astro.ufl.edu

TABLE 1. OBSERVED FLUXES AND MAGNITUDES FOR LENSED IMAGES

Passband	Image A		Image B		Image C		Flux Ratios	
	Flux ( $\mu\text{Jy}$ )	Mag (AB)	Flux( $\mu\text{Jy}$ )	Mag (AB)	Flux( $\mu\text{Jy}$ )	Mag (AB)	B/A	B/C
F606W <sup>a</sup>	<0.29	>25.26	<0.29	>25.26	<0.29	>25.26	...	...
F775W	<0.24	>24.67	<0.24	>24.67	<0.24	>24.67	...	...
F850LP	<0.41	>24.11	<0.41	>24.11	<0.41	>24.11	...	...
J <sub>c</sub>	<1.30	>23.62	<1.30	>23.62	<1.30	>23.62	...	...
K <sub>s</sub>	<5.35	>22.08	<5.35	>22.08	<5.35	>22.08	...	...
3.6 $\mu\text{m}$ <sup>b</sup>	13.6 $\pm$ 0.6	21.06 $\pm$ 0.05	21.0 $\pm$ 1.5	20.59 $\pm$ 0.08	7.4 $\pm$ 1.7	21.73 $\pm$ 0.25	1.54 $\pm$ 0.13	2.84 $\pm$ 0.68
4.5 $\mu\text{m}$	23.4 $\pm$ 0.9	20.47 $\pm$ 0.04	32.7 $\pm$ 1.5	20.11 $\pm$ 0.05	10.6 $\pm$ 1.7	21.34 $\pm$ 0.18	1.40 $\pm$ 0.08	3.08 $\pm$ 0.52
5.8 $\mu\text{m}$	38.4 $\pm$ 1.7	19.94 $\pm$ 0.05	57.9 $\pm$ 1.9	19.49 $\pm$ 0.03	16.8 $\pm$ 1.7	20.84 $\pm$ 0.11	1.51 $\pm$ 0.08	3.45 $\pm$ 0.37
8 $\mu\text{m}$	46.4 $\pm$ 2.5	19.73 $\pm$ 0.06	67.1 $\pm$ 2.5	19.33 $\pm$ 0.04	20.6 $\pm$ 2.5	20.62 $\pm$ 0.13	1.45 $\pm$ 0.09	3.25 $\pm$ 0.41
24 $\mu\text{m}$	390 $\pm$ 20	17.42 $\pm$ 0.05	575 $\pm$ 20	17.00 $\pm$ .04	175 $\pm$ 20	18.29 $\pm$ 0.12	1.47 $\pm$ 0.09	3.29 $\pm$ 0.39

in one of these papers (Bradač et al. 2006, §6 and Fig. 8), and is independently detected as a millimeter source (Wilson et al. 2008a). Here we incorporate new *HST*, *Spitzer*, and Magellan data, in a detailed analysis of this object. The data are presented in §2, and are used in §3 to estimate the redshift, magnification, stellar mass, and star formation rate. In this section we also present evidence for a newly discovered, third image of this galaxy. We summarize our results in §4.

## 2. PHOTOMETRIC DATA AND MEASUREMENTS

We use the combination of *Spitzer* IRAC (Fazio et al. 2004) and MIPS (Rieke et al. 2004), *HST* ACS (Ford et al. 2003), and ground-based near-infrared (NIR) observations to constrain the spectral energy distribution of the multiply imaged source. The subsections below describe the data and photometric analysis associated with each facility.

### 2.1. *Spitzer* IRAC

We originally detected this source as a doubly imaged object in *Spitzer* IRAC data obtained on December 17-18, 2004. The data from this program include imaging in all four IRAC bands (3.6 $\mu\text{m}$ , 4.5 $\mu\text{m}$ , 5.8 $\mu\text{m}$ , and 8 $\mu\text{m}$ ). These data were taken with a cycling dither pattern with medium scale factor and 100s frame time during an 8720s duration Astronomical Observation Request (AOR). The effective exposure times are 4 ks in each filter.

We process the data using MOPEX (Makovoz et al. 2006), with a final pixel scale of 0''.86. Before measuring aperture fluxes, we first use GALFIT (Peng et al. 2002) to model and subtract a cluster elliptical that lies directly between the two lensed images (object #1 in Figure 1), using a nearby, isolated star as the input PSF for GALFIT. The structural parameters for the galaxy are held fixed to values derived using the ACS data (see below), with only the position and magnitude permitted to vary.<sup>4</sup> There is also a star between the two lensed images (object #2 in Fig. 1) that is detected at 3.6 $\mu\text{m}$  and 4.5 $\mu\text{m}$ , but is fainter at these wavelengths than the lensed images. Due to its faintness, we mask this star rather than model it with GALFIT. We also mask two other nearby sources that lie within the background apertures (#3 and #4 in Fig. 1).

<sup>4</sup> The position is permitted to vary at the subpixel level to minimize errors in the subtraction due to residual mis-registration between the images. Fixing the position does not qualitatively alter our results.

We then perform aperture photometry using an aperture of radius 2.4'', with a background annulus extending from 2.4 – 7.2'', applying the point source aperture corrections given in the IRAC Data Handbook.<sup>5</sup> We note that the total magnitude may be underestimated by  $\sim 10\%$  due to the modest spatial extension of the source in the IRAC data, but apply no additional correction for this factor. We measure the flux in an ensemble of off-source apertures to compute the photometric uncertainties. The resultant photometry is given in Table 1 for these two images, which we denote as A and B (Fig. 1 and 2). Image B is brighter than A by a factor of 1.5, with consistent flux ratios in all bands (Fig. 3), as required for a multiply imaged source. The coordinates are  $(\alpha_{2000}, \delta_{2000}) = (06:58:38.0, -55:57:02)$  for image A and  $(\alpha_{2000}, \delta_{2000}) = (06:58:37.1, -55:57:06)$  for image B.

In Table 1 we also present photometry for a newly discovered third image of the galaxy, hereafter denoted as image C (see Fig 1), which is discussed in greater detail in §3.2. The IRAC photometry for image C is obtained in the same fashion as for images A and B, in this case modelling and subtracting two nearby stars and one nearby galaxy (objects #5-7 in Fig. 1).

### 2.2. *Spitzer* MIPS

The MIPS 24 $\mu\text{m}$  data were acquired on November 30, 2007. Observations were taken in small scale photometry mode using a 3 $\times$ 3 raster map with each position offset by half the array. The frame time for individual exposures is 30s.

We process the data using MOPEX, with a final pixel scale of 1''.22. At this wavelength images A, B, and C are all clearly detected. We use APEX (Astronomical Point source EXtractor; Makovoz et al. 2002; Makovoz & Marleau 2005) to perform point source photometry, deblending images A and B. The fluxes of all three lensed images, which are derived via PSF fitting, are reported in Table 1. The quoted uncertainties include uncertainty associated with background subtraction, which dominate over the statistical uncertainties reported by APEX. The MIPS point-source photometry does not suffer from contamination by foreground sources. The spectral energy distributions of cluster ellipticals fall rapidly between 8 $\mu\text{m}$  and 24 $\mu\text{m}$  and the nearby sources modelled at shorter wavelengths are not

<sup>5</sup> See <http://ssc.spitzer.caltech.edu/irac/dh/>. A 2.4'' aperture is the smallest for which corrections are given.

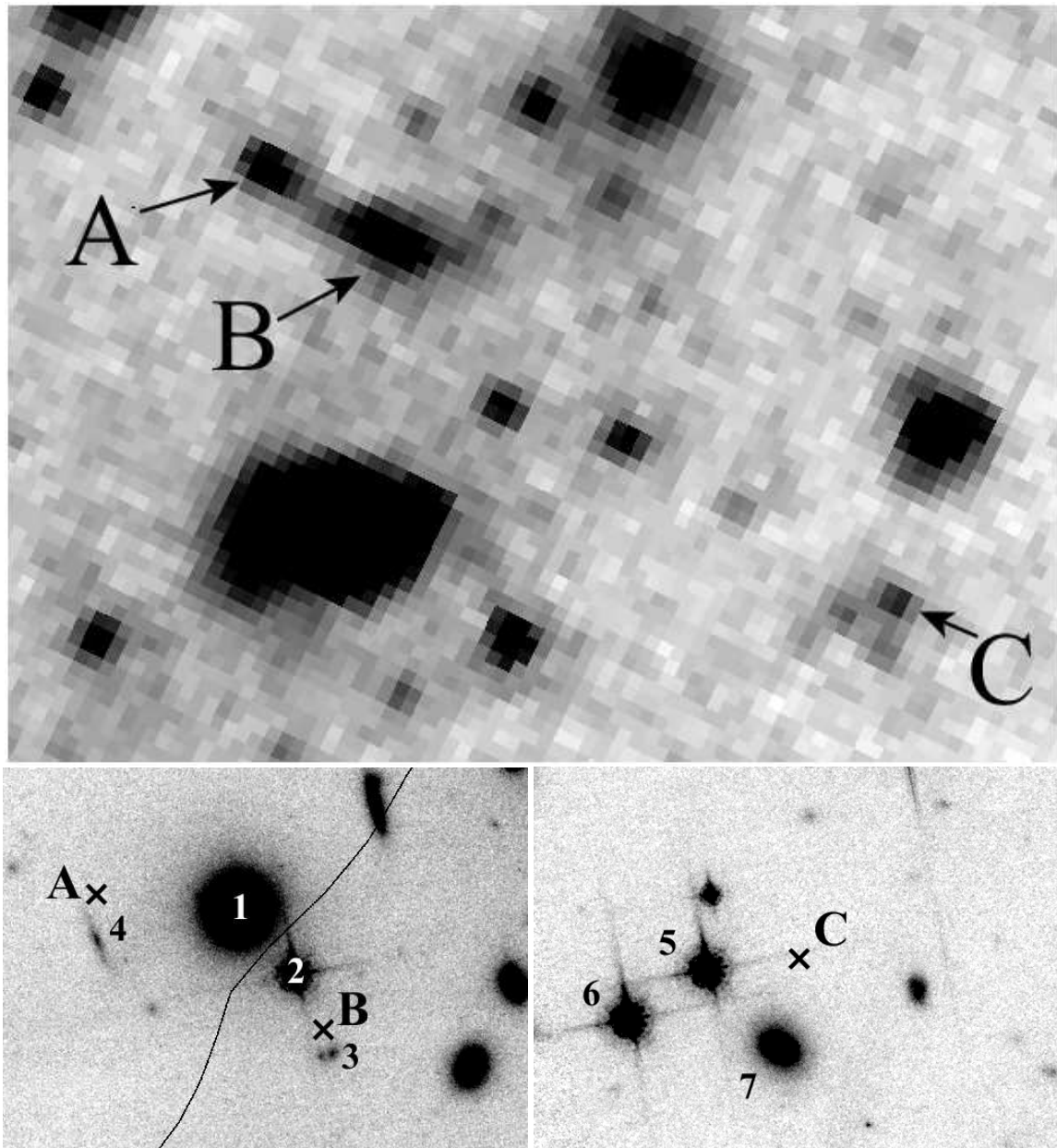


FIG. 1.— *Top*— An  $8\mu\text{m}$  image showing the location of image C relative to images A and B. In this image the galaxy between images A and B has been subtracted for clarity. The field of view is  $65'' \times 50''$ . *Bottom* — F850LP cutouts of the regions surrounding lensed images A and B (left) and image C (right). The crosses denote the locations of each image; the solid curve in the left panel is the critical curve from the  $z = 2.7$  magnification map. The objects detected in the F850LP image that lie closest to the IRAC coordinates for images A and B are numbered 1-4. Object 1 is a cluster elliptical galaxy and object 2 is a star. The two fainter galaxies (3 and 4) are offset from the IRAC detections by  $0.8''$  and  $1.5''$ , whereas the relative astrometry is good to  $0.25''$ , and can thus be excluded as optical counterparts to the lenses. The field of view is  $17'' \times 12''$  in both panels. For all images north is up and east is to the left.

detected at  $24\mu\text{m}$ .

### 2.3. *HST* ACS

We observed the Bullet Cluster with the Advanced Camera for Surveys (ACS) through the F606W, F775W, and F850LP filters. The F606W data were taken on October 21, 2004, with a total exposure time of 4.7ks. The F775W and F850LP data were taken on October 12-13, 2006, with total exposure times of 10.1ks and 12.7ks, respectively. All observations were reprocessed and drizzled to a common coordinate system using custom soft-

ware (Haggles; Marshall et al. 2008, in prep) based upon MultiDrizzle (Koekemoer et al. 2002).

For the *HST* data we perform aperture photometry within  $1.5''$  aperture radii. This aperture size is selected as a tradeoff between two competing factors. Specifically, while smaller apertures yield more stringent lower limits on the magnitude, the aperture size must be sufficiently large to encompass the total flux from each lensed image. Given that IRAC provides the highest resolution data in which the source is detected, our information about the true physical extent of the lensed images is limited. The

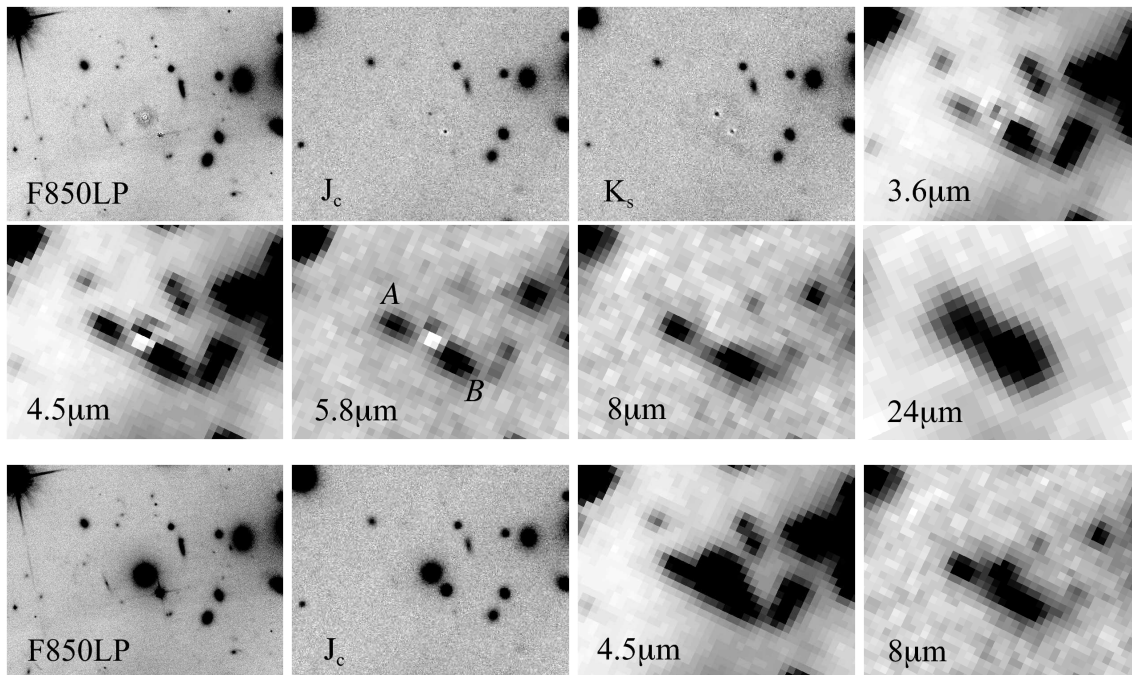


FIG. 2.— Cutout images of the region around the lensed galaxy, in order of increasing wavelength starting with the ACS F850LP data. In the first two rows we show the images used for the photometry after subtraction of contaminant sources using GALFIT. In the last row we show images prior to GALFIT subtraction for a representative sample of wavelengths (F850LP,  $J_c$ ,  $4.5\mu\text{m}$ , and  $8\mu\text{m}$ ). In all panels the field of view is  $34'' \times 26''$ . North is up and east is to the left.

galaxy shows only limited spatial extent at  $3.6\mu\text{m}$ , indicating that a  $1.5''$  aperture is sufficiently large to enclose the total flux in the ACS imaging. Any future higher resolution detection of this object will enable use of smaller apertures and yield improved magnitude limits. As with the IRAC data, we determine the photometric uncertainty using an ensemble of background apertures.

Before measuring aperture fluxes, we again use GALFIT to model and subtract contaminant sources near images A and B. In the *HST* imaging this includes objects #1 and #2. Near image C there are no objects that require subtraction for the *HST* data. We again use a nearby, isolated star as the input PSF for GALFIT, which has the advantage over TinyTim<sup>6</sup> of correctly reproducing the red halo in F850LP (Gilliland & Riess 2002), and we recover consistent structural parameters for the cluster galaxy in all filters (effective radius  $r_e = 0.9''$  and Sersic index  $n = 4.6$ ). We also mask out galaxy #3 in the aperture of image B (Fig. 1). This galaxy cannot be the optical counterpart to the IRAC detection since it is offset from the IRAC detection by  $0.8''$ , whereas the relative astrometry is good to  $0.25''$ . Moreover, both the consistent flux ratios in all IRAC bands for images A and B (see Table 1 and §3) and the location of the critical curve in the lensing model support the interpretation that these are multiple images of the same source. In this case, the relative flux ratio of the two images should also be preserved in the *HST* data, and we would detect the counterimage in the other aperture at high confidence if it were the optical counterpart. For completeness, in Table 2 we provide the *HST* photometry for the objects that are labelled in Figure 1, computed using Source Ex-

tractor.

#### 2.4. Magellan PANIC

We imaged the central region of the Bullet Cluster with the PANIC instrument (Martini et al. 2004) on Magellan on March 06, 2006. Data were obtained in the  $J_c$  and  $K_s$  filters and photometrically calibrated to the 2MASS point source catalog (Skrutskie et al. 2006), with seeing of  $0.55 - 0.6''$  in both bands. Similar to the approach taken with the other data sets, we use GALFIT to fit and subtract off the bright galaxy and star that lie between the locations of images A and B in the IRAC data. We then measure the flux within the same  $1.5''$  apertures employed for the ACS analysis, recovering only upper limits at the positions of all three images.

### 3. ANALYSIS

#### 3.1. Spectral Energy Distribution and Photometric Redshift

In Figure 4 we plot the spectral energy distribution (SED) for each image of the lensed galaxy. Qualitatively the combination of strong upper limits at optical and near-infrared wavelengths coupled with IRAC detections and a strong MIPS detection argue for the galaxy being a dusty starburst at  $z \sim 2$ , with the MIPS  $24\mu\text{m}$  emission being due to the redshifted PAH features. The  $24\mu\text{m}$  emission is difficult to explain if  $z \gtrsim 3$ , while the galaxy should be detected at NIR or optical wavelengths if either the internal extinction is low or the redshift is much below 2.

For a more quantitative answer, we use the photometric redshift code HyperZ (Bolzonella et al. 2000). The input spectral templates are obtained using the Charlot & Bruzual 2007 models (Bruzual 2007) with the

<sup>6</sup> <http://www.stsci.edu/software/tinytim/tinytim.html>

TABLE 2. *HST* PHOTOMETRY FOR OBJECTS NEAR LENSED IMAGES

Fig. 1 ID	F606W (AB)	F775W (AB)	F850LP (AB)	Object Type
1	19.89 ± .02	19.05 ± .03	18.69 ± .03	Galaxy
2	19.79 ± .01	18.95 ± .01	19.17 ± .01	Star
3	24.27 ± .07	23.43 ± .07	23.39 ± .06	Galaxy
4	24.42 ± .07	23.58 ± .08	24.06 ± .08	Galaxy
5	20.34 ± .01	19.50 ± .01	18.75 ± .01	Star
6	19.81 ± .01	18.97 ± .01	18.60 ± .01	Star
7	21.27 ± .03	20.43 ± .03	20.18 ± .03	Galaxy

NOTE. — In this Table we quote Source Extractor AUTO magnitudes. The uncertainties are calculated using artificial stars and galaxies.

Padova 1994 evolutionary tracks (Bertelli et al. 1994) and a Chabrier (2003) mass function. The templates are defined to have star formation histories identical to the default synthetic templates provided with *HyperZ*,<sup>7</sup> and a Calzetti et al. (2000) extinction law is employed.

Since these stellar templates do not include PAH emission, for the photometric redshifts we fit only the data shortward of  $10\mu\text{m}$ . *HyperZ* yields a best fit redshift  $z = 2.72^{+0.19}_{-0.32}$  for image A (90% confidence;  $\chi^2_\nu = 0.5$ ). A small secondary peak in the redshift probability distribution is observed at  $z = 5$  (Fig. 5); however, this redshift is implausible because of the high observed flux at  $24\mu\text{m}$ . An analysis of image B yields a similar redshift  $z = 2.62^{+0.14}_{-0.22}$  ( $\chi^2_\nu = 0.97$ ) with no secondary peak. In Bradač et al. (2006) we speculated that the source might be at  $z > 6$ , but this possibility is now excluded at high confidence ( $\Delta\chi^2 > 8$ ). The best fit spectral template (Fig. 4) corresponds to a dusty starburst galaxy with  $A_V = 3.3^{+2.2}_{-0.8}$  (90%) and an age of  $< 30$  Myr. As can be seen in the figure, the robustness of the photometric redshift is largely due to the fact that the IRAC data span the  $1.6\mu\text{m}$  bump at this redshift.

At the best-fit redshift the  $7.7\mu\text{m}$  and  $8.6\mu\text{m}$  PAH features (blended in this spectrum) are redshifted beyond the  $24\mu\text{m}$  window, in which case the observed  $24\mu\text{m}$  emission is dominated by the  $6.24\mu\text{m}$  PAH feature. In a concurrent program (Wilson et al. 2008a) have also identified this galaxy as a bright millimeter source, and obtain a consistent redshift ( $z = 2.7$ ) via an empirical relation for SMGs between redshift and IRAC colors.

### 3.2. Magnification and Additional Images

The magnification map was obtained from the strong (information from multiply imaged systems) and weak (measuring distortion of background galaxies) gravitational lensing data. It is the same reconstruction as in Bradač et al. (2006). It is performed on a pixelized grid and does *not* assume a specific form of the underlying gravitational potential. At the location of image A we compute a magnification  $|\mu| \sim 25$  and at image B we obtain  $|\mu| \sim 50$  for a galaxy at  $z = 2.7$ . The critical curve

<sup>7</sup> These templates have exponentially declining star formation rates with  $\tau = 1, 2, 3, 5, 15, 30$  Gyr for E, S0, Sa, Sb, Sc, and Sd galaxies, respectively. There is also a starburst template that corresponds to a single, instantaneous burst model. For all templates the metallicity is solar; however, Bolzonella et al. (2000) demonstrated that the redshift determination is not strongly dependent upon metallicity.

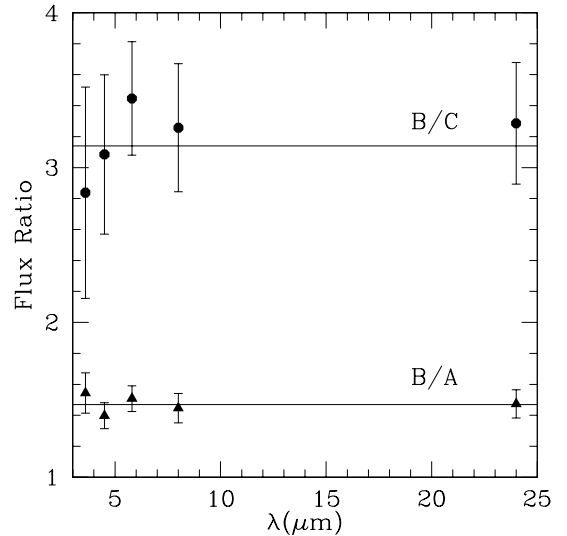


FIG. 3.— Flux ratios for the three images as a function of wavelength. The solid lines correspond to the weighted mean flux ratios, including data at all wavelengths. The observed flux ratios at different wavelengths are consistent to within the photometric uncertainties. For B/A (triangles) and B/C (circles) these mean values are  $1.47 \pm 0.06$  and  $3.18 \pm 0.23$  respectively. The flux ratio for A/C, which is not plotted, is  $2.16 \pm 0.18$ .

(points of infinite magnification) passes between images A and B (see Fig.1) – their parity is reversed – supporting the hypothesis that A and B are indeed multiple images of the same source. These magnifications change by  $< 20\%$  within the range of allowed photometric redshifts (90% confidence interval, see §3.1). The measured flux ratio of the two images is  $1.47 \pm 0.05$  which is similar to the flux ratio of  $\sim 2$  given by our lens model. In the subsequent discussion we will quote the stellar mass and star formation rate in terms of  $(\mu_A/25)^{-1}$  to reflect the inherent magnification uncertainty.

Given both lensing model and positions of images A and B, we can search for additional images of this source. We identified image C (Figure 1) at  $(\alpha_{2000}, \delta_{2000}) = (06:58:33.4, -55:57:29)$  using the same initial lens model, which does not include information from images A and B of this object. The photometry for image C, described in §2, indicates that this image is a factor of 2.2 fainter than image A, while our lens model predicts a factor of four. Given the uncertainties these images are still consistent with being multiple images. The best-fit photometric redshift derived for this source is  $z = 2.82^{+0.18}_{-0.20}$ .

### 3.3. Stellar Mass

To estimate the stellar mass we use the code *kcorrect* (Blanton & Roweis 2007), which fits a linear combination of Bruzual & Charlot (2003) templates based upon Padova 1994 isochrones and spanning a range in metallicity (0.005 – 2.5 times solar) and age (1 Myr to 13.75 Gyr). The required inputs are the photometric redshift from *HyperZ* and the IRAC photometry, reddening corrected using the  $A_V$  from *HyperZ* and the Calzetti et al. (2000) reddening law. In this analysis and §3.5 we focus upon image A, but note that equivalent results hold for image B. For  $z = 2.72$  and  $A_V = 3.3$  we

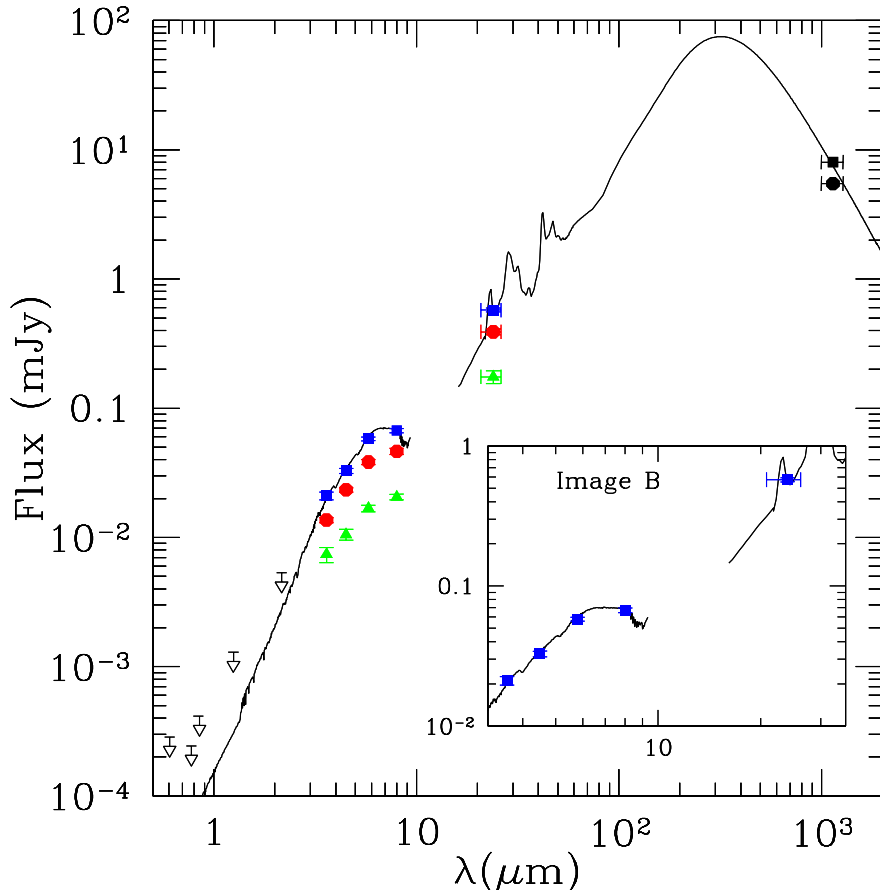


FIG. 4.— Spectral energy distribution for the galaxy. The solid points correspond to the observed fluxes for images A (circles), B (squares), and C (triangles), while the open arrows correspond to the  $5\sigma$  upper limits at optical and NIR wavelengths. The solid circles at 1.1 mm are the AzTEC data from Wilson et al. (2008), where we have split their observed flux using the flux ratio derived for images A and B (see Fig. 3). Horizontal error bars on the  $24\mu\text{m}$  data points denote the width of the filter, and for the AzTEC data correspond approximately to the system bandpass (Wilson et al. 2008b). The solid curve at  $\lambda < 10\mu\text{m}$  is the best-fit spectrum returned by *HyperZ* for image B, which corresponds to a starburst galaxy. The solid curve redward of  $10\mu\text{m}$  is the template from Chary & Elbaz (2001) that best fits the  $24\mu\text{m}$  flux for image A assuming  $\mu_A = 25$ . This template is redshifted to  $z = 2.7$  and rescaled to image B using the observed flux ratio of the two images (Fig. 3). Note that the AzTEC data, while not included in the fit, is fully consistent with this model. The inset zooms in on the wavelength regime covered by *Spitzer*, showing only the photometry for image B for clarity.

obtain a stellar mass  $M_* = 1.5 \times 10^{10} (\mu_A/25)^{-1} M_\odot$ .<sup>8</sup> Thus, we find that this lensed galaxy is massive – similar in mass to LIRGs at lower redshift (Caputi et al. 2006).

### 3.4. Presence of an AGN

In the sections above we have determined the redshift and stellar mass assuming that the observed SED is dominated by stars. It is true however that dusty starbursts and active galactic nuclei are difficult to discriminate at the source redshift (e.g., see Barmby et al. 2006).

The simplest discriminator between the two contributors is spatial extent – any spatially extended emission must be stellar rather than due to an AGN. A visual inspection of Figure 2 demonstrates that the IRAC images do exhibit a modest extension perpendicular to the critical curve, arguing that the flux is not purely from an AGN. Next, we consider the *Chandra* observations to

search for evidence of AGN activity. We find that the lensed source is a non-detection in our 500 ks exposure ( $f < 3.6 \times 10^{-16} \text{ erg s}^{-1} \text{ cm}^{-2}$  unabsorbed,  $3\sigma$ , for 0.5-2 keV). Comparing with the local X-ray to mid-IR relations of Krabbe et al. (2001), we find that a local Seyfert galaxy of comparable mid-IR luminosity should be more than a factor of 10 brighter than this limit, whereas non-detection is consistent with the expected relation for a starburst galaxy. While neither of the above arguments exclude an additional contribution from a central AGN, they do argue that we are not looking at a purely AGN spectrum.

Given the  $24\mu\text{m}$  data, we can also consider whether this source, which is also a millimeter galaxy (Wilson et al. 2008a), has mid-IR colors consistent with a starburst or AGN. Comparing with the distribution of  $24\mu\text{m}$ - $8\mu\text{m}$  vs.  $8\mu\text{m}$ - $4.5\mu\text{m}$  colors for SMGs in Pope et al. (2008), we find that the designation is ambiguous. The source lies close to, but outside the regime defined in Pope et al. (2008) for starburst galaxies, arguing that the observed SED may be a composite with

<sup>8</sup> As noted by Maraston et al. (2006), templates that include the contribution of TP-AGB stars to the spectrum can yield stellar masses roughly a factor of two lower. These templates are not currently implemented in *kcorrect*.

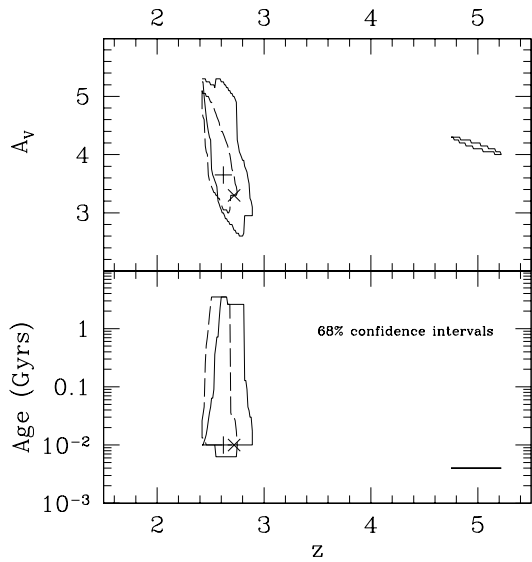


FIG. 5.— The 68% confidence intervals from *HyperZ* in the redshift-extinction and redshift-age planes. The solid curves denote the confidence intervals for image A; the dashed curves are for image B. The crosses (plus signs) denote the values corresponding to the minimum  $\chi^2$  for image A (B). There is a small secondary peak in the solutions for image A at  $z = 5$ .

AGN and starburst contributions.

### 3.5. Star Formation Rate

The only means of estimating the star formation rate with the existing data is via the strength of the PAH emission. There are two main caveats to this approach. First, any AGN contribution will bias our estimate of the star formation rate. Second, there exists large scatter in the relation between  $8\mu\text{m}$  emission and star formation as traced by other methods (Calzetti 2008).

Keeping the above caveats in mind, we cautiously proceed with deriving a rough estimate of the star formation rate. To do so, we first convert the observed  $24\mu\text{m}$  luminosity to  $L_{IR}$  and then use the local Kennicutt (1998) relation to convert  $L_{IR}$  to star formation rate. Using the templates and code from Chary & Elbaz (2001) to fit the  $24\mu\text{m}$  flux, assuming  $z = 2.7$ , we derive a best-fit  $L_{IR} = 5 \times 10^{11} (\mu_A/25)^{-1} L_\odot$ . The corresponding implied star formation rate is  $\text{SFR} \sim 90 (\mu_A/25)^{-1} M_\odot \text{ yr}^{-1}$ . As a consistency check, we also derive the rest-frame  $8\mu\text{m}$  luminosity and convert to  $L_{IR}$  using  $L_{8\mu\text{m}}/L_{IR} = 10$ , consistent with recent results from Rigby et al. (2008) based upon a combination of local and  $z \sim 2$  galaxies. To derive the rest-frame  $8\mu\text{m}$  we use the same spectral index correction ( $\alpha = 2.296$ ) as in Dey et al. (2008). This approach yields a qualitatively consistent total luminosity,  $L_{IR} \sim 3 \times 10^{11} (\mu_A/25)^{-1} L_\odot$ .

In Figure 4 we overlay the best-fit Chary & Elbaz (2001) template for image B, redshifted to  $z = 2.7$ , at wavelengths redward of  $10\mu\text{m}$ . If the magnification is a factor of two lower than our canonical value, which boot-strap simulations indicate is the maximum by which we

may be overestimating  $\mu_A$ , this galaxy would lie at the borderline between LIRG and ULIRG luminosity. From their AzTEC millimeter data, Wilson et al. (2008a) also estimate  $L_{IR} = 10^{11} - 10^{12} L_\odot$  for this source. The estimated specific star formation rate for this galaxy,  $\text{SFR} \approx 5 \text{ Gyr}^{-1}$ , is comparable to that of similar mass BM/BX galaxies at  $z = 1.5 - 2.6$  (Reddy et al. 2006).

## 4. DISCUSSION

We have presented confirmation observations for a multiply imaged source behind the Bullet Cluster, and identified a third, previously unknown image. From our multiwavelength imaging we argue that the source is most consistent with being a dusty ( $A_V \sim 3.3$ ), strongly star-forming galaxy at  $z \sim 2.7$ . At this redshift our mass model for the cluster core indicates that the galaxy is highly magnified ( $\mu_A \sim 25$ ), implying a large intrinsic stellar mass of  $M_* \sim 2 \times 10^{10} M_\odot$ . We estimate a star formation rate of  $\sim 90 M_\odot \text{ yr}^{-1}$  based upon the observed flux in the  $24\mu$  band, which we assume to be dominated by emission from redshifted PAH features.

The estimated intrinsic infrared luminosity of this galaxy ( $5 \times 10^{11} L_\odot$ ) qualifies it as a luminous infrared galaxy (LIRG), fainter than the ULIRGs typically studied at this epoch. The galaxy is also known to be an exceptionally bright SMG (13.5 mJy at 1.1 mm, Wilson et al. 2008a), and thus may be an ideal system for studying the connection between different classes of infrared sources at lower intrinsic luminosity than has previously been possible for this epoch. We anticipate that the galaxy will be detected in scheduled deep *HST* NICMOS observations, providing information on the spatial extent of the lensed images.

The Bullet Cluster, due to its large lensing cross-section, provides an optimal environment in which to identify lensed galaxies such as the one presented here. However, even in this rare, massive cluster merger, we detected only one lensed LIRG. This result highlights that the prospects are not good for finding large samples of  $z \sim 2$ , gravitationally-lensed LIRGS. It is for this reason that each case must be highlighted and exploited.

AHG thanks Ranga-Ram Chary, Arjun Dey, Jean-Paul Kneib, and Alexandra Pope, and Grant Wilson for constructive discussions related to this work, Stéphane Charlot and Gustavo Bruzual for providing access to the Charlot & Bruzual 2007 models, and the anonymous referee for comments that significantly improved the manuscript. The authors acknowledge support for this work from NASA/HST grants HST-GO-10200, HST-GO-10863, and HST-GO-11099, as well as NASA/Spitzer grant 1319141. MB also acknowledges support from NASA through Hubble Fellowship grant # HST-HF-01206.01 awarded by the Space Telescope Science Institute.

*Facilities:* HST (ACS), Spitzer (IRAC,MIPS), CXO (ACIS), Magellan:Baade (PANIC)

## REFERENCES

- Barmby, P., Alonso-Herrero, A., Donley, J. L., Egami, E., Fazio, G. G., Georgakakis, A., Huang, J.-S., Laird, E. S., Miyazaki, S., Nandra, K., Park, S. Q., Pérez-González, P. G., Rieke, G. H., Rigby, J. R., & Willner, S. P. 2006, *ApJ*, 642, 126
- Bertelli, G., Bressan, A., Chiosi, C., Fagotto, F., & Nasi, E. 1994, *A&AS*, 106, 275
- Blanton, M. R. & Roweis, S. 2007, *AJ*, 133, 734

- Bolzoniella, M., Miralles, J.-M., & Pelló, R. 2000, *A&A*, 363, 476
- Bradač, M., Clowe, D., Gonzalez, A. H., Marshall, P., Forman, W., Jones, C., Markevitch, M., Randall, S., Schrabback, T., & Zaritsky, D. 2006, *ApJ*, 652, 937
- Bruzual, A. G. 2007, in *IAU Symposium*, Vol. 241, IAU Symposium, ed. A. Vazdekis & R. F. Peletier, 125–132
- Bruzual, G. & Charlot, S. 2003, *MNRAS*, 344, 1000
- Calzetti, D. 2008, *ArXiv e-prints*, 801
- Calzetti, D., Armus, L., Bohlin, R. C., Kinney, A. L., Koornneef, J., & Storchi-Bergmann, T. 2000, *ApJ*, 533, 682
- Caputi, K. I., Dole, H., Lagache, G., McLure, R. J., Puget, J.-L., Rieke, G. H., Dunlop, J. S., Le Floch, E., Papovich, C., & Pérez-González, P. G. 2006, *ApJ*, 637, 727
- Chabrier, G. 2003, *PASP*, 115, 763
- Chary, R. & Elbaz, D. 2001, *ApJ*, 556, 562
- Clowe, D., Bradač, M., Gonzalez, A. H., Markevitch, M., Randall, S. W., Jones, C., & Zaritsky, D. 2006, *ApJ*, 648, L109
- Clowe, D., Gonzalez, A., & Markevitch, M. 2004, *ApJ*, 604, 596
- Daddi, E., Dickinson, M., Chary, R., Pope, A., Morrison, G., Alexander, D. M., Bauer, F. E., Brandt, W. N., Giavalisco, M., Ferguson, H., Lee, K.-S., Lehmer, B. D., Papovich, C., & Renzini, A. 2005, *ApJ*, 631, L13
- Dey, A., Soifer, B. T., Desai, V., Brand, K., LeFloch, E., Brown, M. J., Jannuzi, B. T., Armus, L., Bussmann, S., Brodwin, M., Bian, C., Eisenhardt, P., Higdon, S., Weedman, D., & Willner, S. 2008, *ArXiv e-prints*, 801
- Dickinson, M., Papovich, C., Ferguson, H. C., & Budavári, T. 2003, *ApJ*, 587, 25
- Dye, S., Eales, S. A., Aretxaga, I., Serjeant, S., Dunlop, J. S., Babbidge, T. S. R., Chapman, S. C., Cirasuolo, M., Clements, D. L., Coppin, K. E. K., Dunne, L., Egami, E., Farrah, D., Ivison, R. J., van Kampen, E., Pope, A., Priddey, R., Rieke, G. H., Schael, A. M., Scott, D., Simpson, C., Takagi, T., Takata, T., & Vaccari, M. 2008, *ArXiv e-prints*, 802
- Fazio, G. G., Hora, J. L., Allen, L. E., Ashby, M. L. N., Barmby, P., Deutsch, L. K., Huang, J.-S., Kleiner, S., Marengo, M., Megeath, S. T., Melnick, G. J., Pahre, M. A., Patten, B. M., Polizotti, J., Smith, H. A., Taylor, R. S., Wang, Z., Willner, S. P., Hoffmann, W. F., Pipher, J. L., Forrest, W. J., McMurty, C. W., McCreight, C. R., McKelvey, M. E., McMurray, R. E., Koch, D. G., Moseley, S. H., Arendt, R. G., Mentzell, J. E., Marx, C. T., Losch, P., Mayman, P., Eichhorn, W., Krebs, D., Jhabvala, M., Gezari, D. Y., Fixsen, D. J., Flores, J., Shakoorzadeh, K., Jungo, R., Hakun, C., Workman, L., Karpati, G., Kichak, R., Whitley, R., Mann, S., Tollestrup, E. V., Eisenhardt, P., Stern, D., Gorjian, V., Bhattacharya, B., Carey, S., Nelson, B. O., Glaccum, W. J., Lacy, M., Lowrance, P. J., Laine, S., Reach, W. T., Stauffer, J. A., Surace, J. A., Wilson, G., Wright, E. L., Hoffman, A., Domingo, G., & Cohen, M. 2004, *ApJS*, 154, 10
- Ford, H. C., Clampin, M., Hartig, G. F., Illingworth, G. D., Sirianni, M., Martel, A. R., Meurer, G. R., McCann, W. J., Sullivan, P. C., Bartko, F., Benitez, N., Blakeslee, J., Bouwens, R., Broadhurst, T., Brown, R. A., Burrows, C. J., Campbell, D., Cheng, E. S., Feldman, P. D., Franx, M., Golimowski, D. A., Gronwall, C., Kimble, R. A., Krist, J. E., Lesser, M. P., Magee, D., Miley, G., Postman, M., Rafal, M. D., Rosati, P., Sparks, W. B., Tran, H. D., Tsvetanov, Z. I., Volmer, P., White, R. L., & Woodruff, R. A. 2003, in *Presented at the Society of Photo-Optical Instrumentation Engineers (SPIE) Conference*, Vol. 4854, *Future EUV/UV and Visible Space Astrophysics Missions and Instrumentation*. Edited by J. Chris Blades, Oswald H. W. Siegmund. *Proceedings of the SPIE*, Volume 4854, pp. 81–94 (2003)., ed. J. C. Blades & O. H. W. Siegmund, 81–94
- Gilliland, R. L. & Riess, A. 2002, in *The 2002 HST Calibration Workshop : Hubble after the Installation of the ACS and the NICMOS Cooling System*, ed. S. Arribas, A. Koekemoer, & B. Whitmore, 61–
- Kennicutt, Jr., R. C. 1998, *ApJ*, 498, 541
- Knudsen, K. K., van der Werf, P. P., & Kneib, J.-P. 2008, *MNRAS*, 384, 1611
- Koekemoer, A. M., Fruchter, A. S., Hook, R. N., & Hack, W. 2002, in *The 2002 HST Calibration Workshop : Hubble after the Installation of the ACS and the NICMOS Cooling System*, ed. S. Arribas, A. Koekemoer, & B. Whitmore, 337–
- Krabbe, A., Böker, T., & Maiolino, R. 2001, *ApJ*, 557, 626
- Le Floch, E., Papovich, C., Dole, H., Bell, E. F., Lagache, G., Rieke, G. H., Egami, E., Pérez-González, P. G., Alonso-Herrero, A., Rieke, M. J., Blaylock, M., Engelbracht, C. W., Gordon, K. D., Hines, D. C., Misselt, K. A., Morrison, J. E., & Mould, J. 2005, *ApJ*, 632, 169
- Lilly, S. J., Le Fevre, O., Hammer, F., & Crampton, D. 1996, *ApJ*, 460, L1+
- Madau, P., Ferguson, H. C., Dickinson, M. E., Giavalisco, M., Steidel, C. C., & Fruchter, A. 1996, *MNRAS*, 283, 1388
- Makovoz, D. & Marleau, F. R. 2005, *PASP*, 117, 1113
- Makovoz, D., Moshir, M., Laher, R., & Marsh, K. 2002, in *Astronomical Society of the Pacific Conference Series*, Vol. 281, *Astronomical Data Analysis Software and Systems XI*, ed. D. A. Bohlender, D. Durand, & T. H. Handley, 417–
- Makovoz, D., Roby, T., Khan, I., & Booth, H. 2006, in *Presented at the Society of Photo-Optical Instrumentation Engineers (SPIE) Conference*, Vol. 6274, *Advanced Software and Control for Astronomy*. Edited by Lewis, Hilton; Bridger, Alan. *Proceedings of the SPIE*, Volume 6274, pp. 62740C (2006).
- Maraston, C., Daddi, E., Renzini, A., Cimatti, A., Dickinson, M., Papovich, C., Pasquali, A., & Pirzkal, N. 2006, *ApJ*, 652, 85
- Markevitch, M., Gonzalez, A. H., Clowe, D., Vikhlinin, A., Forman, W., Jones, C., Murray, S., & Tucker, W. 2004, *ApJ*, 606, 819
- Markevitch, M., Gonzalez, A. H., David, L., Vikhlinin, A., Murray, S., Forman, W., Jones, C., & Tucker, W. 2002, *ApJ*, 567, L27
- Martini, P., Persson, S. E., Murphy, D. C., Birk, C., Sheckman, S. A., Gunnels, S. M., & Koch, E. 2004, in *Presented at the Society of Photo-Optical Instrumentation Engineers (SPIE) Conference*, Vol. 5492, *Ground-based Instrumentation for Astronomy*. Edited by Alan F. M. Moorwood and Iye Masanori. *Proceedings of the SPIE*, Volume 5492, pp. 1653-1660 (2004)., ed. A. F. M. Moorwood & M. Iye, 1653–1660
- Peng, C. Y., Ho, L. C., Impey, C. D., & Rix, H.-W. 2002, *AJ*, 124, 266
- Pérez-González, P. G., Rieke, G. H., Egami, E., Alonso-Herrero, A., Dole, H., Papovich, C., Blaylock, M., Jones, J., Rieke, M., Rigby, J., Barmby, P., Fazio, G. G., Huang, J., & Martin, C. 2005, *ApJ*, 630, 82
- Pope, A., Chary, R.-R., Alexander, D. M., Armus, L., Dickinson, M., Elbaz, D., Frayer, D., Scott, D., & Teplitz, H. 2008, *ApJ*, 675, 1171
- Randall, S. W., Markevitch, M., Clowe, D., Gonzalez, A. H., & Bradač, M. 2007, *ArXiv e-prints*, 704
- Reddy, N. A. & Steidel, C. C. 2004, *ApJ*, 603, L13
- Reddy, N. A., Steidel, C. C., Fadda, D., Yan, L., Pettini, M., Shapley, A. E., Erb, D. K., & Adelberger, K. L. 2006, *ApJ*, 644, 792
- Reddy, N. A., Steidel, C. C., Pettini, M., Adelberger, K. L., Shapley, A. E., Erb, D. K., & Dickinson, M. 2008, *ApJS*, 175, 48
- Rieke, G. H., Young, E. T., Engelbracht, C. W., Kelly, D. M., Low, F. J., Haller, E. E., Beeman, J. W., Gordon, K. D., Stansberry, J. A., Misselt, K. A., Cadien, J., Morrison, J. E., Rivlis, G., Latter, W. B., Noriega-Crespo, A., Padgett, D. L., Stapelfeldt, K. R., Hines, D. C., Egami, E., Muzerolle, J., Alonso-Herrero, A., Blaylock, M., Dole, H., Hinz, J. L., Le Floch, E., Papovich, C., Pérez-González, P. G., Smith, P. S., Su, K. Y. L., Bennett, L., Frayer, D. T., Henderson, D., Lu, N., Masci, F., Pesenson, M., Rebull, L., Rho, J., Keene, J., Stolovy, S., Wachter, S., Wheaton, W., Werner, M. W., & Richards, P. L. 2004, *ApJS*, 154, 25
- Rigby, J. R., Marcillac, D., Egami, E., Rieke, G. H., Richard, J., Kneib, J.-P., Fadda, D., Willmer, C. N. A., Borys, C., van der Werf, P. P., Pérez-González, P. G., Knudsen, K. K., & Papovich, C. 2008, *ApJ*, 675, 262
- Rudnick, G., Rix, H., Franx, M., Labbé, I., Blanton, M., Daddi, E., Förster Schreiber, N. M., Moorwood, A., Röttgering, H., Trujillo, I., van de Wel, A., van der Werf, P., van Dokkum, P. G., & van Starckenburg, L. 2003, *ApJ*, 599, 847
- Skrutskie, M. F., Cutri, R. M., Stiening, R., Weinberg, M. D., Schneider, S., Carpenter, J. M., Beichman, C., Capps, R., Chester, T., Elias, J., Huchra, J., Liebert, J., Lonsdale, C., Monet, D. G., Price, S., Seitzer, P., Jarrett, T., Kirkpatrick, J. D., Gizis, J. E., Howard, E., Evans, T., Fowler, J., Fullmer, L., Hurt, R., Light, R., Kopan, E. L., Marsh, K. A., McCallon, H. L., Tam, R., Van Dyk, S., & Wheelock, S. 2006, *AJ*, 131, 1163
- Valiante, E., Lutz, D., Sturm, E., Genzel, R., Tacconi, L. J., Lehnert, M. D., & Baker, A. J. 2007, *ApJ*, 660, 1060
- Wilkins, S. M., Trentham, N., & Hopkins, A. M. 2008, *MNRAS*, 385, 687



- Wilson, G. W., Aretxaga, I., Hughes, D., Ezawa, H., Austermann, J. E., Doyle, S., Hernandez-Curiel, I., Kawabe, R., Kitayama, T., Kohno, K., Kuboi, A., Matsuo, H., Mauskopf, P. D., Murakoshi, Y., Montana, A., Natarajan, P., Oshima, T., Ota, N., Perera, T., Rand, J., Scott, K. S., Tanaka, K., Tsuboi, M., Williams, C. C., & Yun, M. S. 2008a, ArXiv e-prints, 803
- Wilson, G. W., Austermann, J. E., Perera, T. A., Scott, K. S., Ade, P. A. R., Bock, J. J., Glenn, J., Golwala, S. R., Kim, S., Kang, Y., Lydon, D., Mauskopf, P. D., Predmore, C. R., Roberts, C. M., Souccar, K., & Yun, M. S. 2008b, MNRAS, 386, 807
- Yan, L., Chary, R., Armus, L., Teplitz, H., Helou, G., Frayer, D., Fadda, D., Surace, J., & Choi, P. 2005, ApJ, 628, 604